On the observability of mesoscopic or macroscopic quantum coherence of domain walls in magnetic insulators

1994 J. Phys.: Condens. Matter 6 7565

(http://iopscience.iop.org/0953-8984/6/37/011)

J. Phys.: Condens. Matter 6 (1994) 7565–7579. Printed in the UK

On the observability of mesoscopic or macroscopic quantum coherence of domain walls in magnetic insulators

Frank Gaitan

Department of Physics, University of British Columbia, 6224 Agriculture Road, Vancouver, British Columbia, Canada, V6T 1Z1

Received 24 March 1994, in final form 8 June 1994

Abstract. Results are presented of a numerical calculation of the tunnelling gap for a domain wall moving in the double-well potential of a pair of voids in a magnetic insulator. Both symmetric and asymmetric double-well potentials are considered. It is found that the prospect for observing domain wall quantum coherence on a mesoscopic or macroscopic scale appears highly unlikely.

1. Introduction

There has been a great deal of interest recently in the prospect that magnetic systems might provide a new setting in which to observe a macroscopic degree of freedom behaving quantum mechanically [1]. To date, the magnetic systems considered are (i) magnetic grains [2, 3, 4, 5, 6] and (ii) solitons in magnetic systems (particularly 180° Bloch walls) [1, 7, 8, 9, 10, 11]. Attention has focused on macroscopic quantum tunnelling since the conditions necessary for its observation appear the most favourable [12]. Arguably, of more fundamental interest is macroscopic quantum coherence (MQC) because of its connections with quantum measurement theory [13]. In MQC the macroscopic object tunnels *periodically* through the central barrier of a double-well potential (DWP). This effect is a direct consequence of the quantum state of the object being in a coherent linear superposition of macroscopically distinguishable states, and it is this aspect of MQC that connects it to the Schrödinger cat paradox [14] and to quantum measurement theory.

In this paper we will examine quantum coherence (QC) for a 180° Bloch wall (we suppress the '180°' below) moving in the double-well potential due to a pair of voids present in a uniaxial magnetic insulator with quality factor $Q = K/2\pi M^2 \gg 1$ (K = magnetic anisotropy constant, M = spontaneous magnetization) at $T = 0$ [15]. Because of the restriction on Q, demagnetization effects are small so that the voids will not alter significantly the Bloch wall configuration of the magnetization (see appendix A). It is well known that dissipative effects on domain walls in magnetic insulators are weak as long as $k_B T \ll \Delta_0$ (Δ_0 is the bulk magnon gap). Thus our system, under the conditions assumed, is expected to have weak dissipation which allows an iterative approach to treating the effects of dissipation. At stage 1 of the calculation, we do not include the effects of dissipation and go ahead and calculate the tunnelling gap. From this we study the nature of quantum coherence in the case where only non-dissipative couplings to the environment are considered. Qualitatively, there are only two results possible at the end of stage 1, either (i) the natures of the non-dissipative couplings are such that macroscopic quantum coherence is

0953-8984/94/377565+15$19.50

possible or (ii) they are such that macroscopic quantum coherence is not possible. If case (i) is found at the end of stage 1, then we must go on to stage 2 of the calculation and include the effects of dissipation to see how such effects influence the nature of the macroscopic quantum coherence. This could be done along the lines of the work of Leggett *et al* [16]. As the principle source of dissipation at these temperatures for a domain wall in a magnetic insulator is due to magnons [8] (though see [17]), which produce ohmic dissipation with $\alpha \ll 1$ (at the temperatures considered), it is expected that dissipation would lead to damped oscillations (damped quantum coherence) for zero or very weak bias. One would then have to re-examine the effects of the non-dissipative couplings to the environment to fully assess the effects of the environment on macroscopic quantum coherence. If instead, case (ii) is found at the end of stage 1, then macroscopic quantum coherence is already destroyed by non-dissipative effects. As shown by Leggett and co-workers, dissipative effects (depending on the details of the dissipative couplings) will either destroy the oscillations (that are quantum coherent), or else damp them. Thus, if case (ii) is found at the end of stage 1, the iteration can cease and the calculation is complete as including dissipation at stage 2 will not restore quantum coherence. As we will see below, the result of stage 1 of this iterative calculation is case (ii)—macroscopic quantum coherence is destroyed by non-dissipative effects. Thus it is unnecessary to carry out stage 2 of the calculation as dissipation will not act to restore macroscopic quantum coherence. Thus we want to stress that although the numerical calculation to be presented below does not include dissipation, the nature of the results obtained (i.e. quantum coherence is destroyed by non-dissipative effects) are such that including dissipative effects will not alter our conclusion. In fact, such effects will act to strengthen our result.

Below we calculate numerically the ground- (first-excited-) state energy E_0 (E_1) (from which the tunnelling gap is $\Delta_0 = E_1 - E_0$) for: (i) identical voids leading to a symmetric double-well potential for various wall sizes N (the number of spins in the wall) and void separations L; and (ii) non-identical voids leading to an asymmetric double-well potential for varying degrees of asymmetry (for a particular choice of N and L). We find that observation of quantum coherence on either a macroscopic or mesoscopic scale appears unlikely. For macroscopic QC ($N \geqslant 10^4$), weak stray magnetic fields introduce a bias into the gap which masks Δ_0 except for void separations very close to the value at which the central barrier disappears. At these separations, the tunnelling gap varies on a length scale that is less than the coarse-graining length scale. One would expect that the experimentally relevant gap would be a coarse-grained average which is seen to be less than the bias and so unobservable. For mesoscopic QC ($N \simeq 10^2$–10^3), although the bias introduced by a stray magnetic field is quite small, the slightest degree of asymmetry in the voids is sufficient to pin the wall to the larger of the two voids. The difficulty here is that an adequately large tunnelling gap requires a very small central barrier which is destroyed by the slightest difference in the voids. For spherical voids, we find that pinning of the wall can be avoided only when the difference in the radii is much less than the coarse-graining length scale. Averaging the effects of asymmetry over the coarse-graining length scale leads one to conclude that a real mesoscopic wall will likely be pinned by asymmetry. Thus even in the dissipationless approximation, one expects that observation of quantum coherence on any scale larger than microscopic appears unlikely due to the severe tolerances imposed on the experimental situation. As discussed above, given the nature of this result, it is unnecessary to extend the calculation to include dissipative effects as they will not act to restore QC.

The organization of this paper is as follows. Section 2 is concerned with issues that lead us to the Hamiltonian we will use to examine domain wall QC. In section 3 we describe the

numerical calculation and in the following section we present our results and their analysis. In section 5 we summarize what has been found and make closing remarks. Two appendices are included in which (i) the effect of a void (in the magnetic insulator) on the Bloch wall structure is examined (appendix A) and (ii) a derivation of the pinning potential is given (appendix B).

2. Preliminaries

The system of interest is a magnetic insulator which is a lattice of spins (with lattice constant l_0) coupled to each other via the exchange and dipole–dipole interactions, and to the underlying lattice via the anisotropy interaction which is assumed to be uniaxial with easy axis along $\hat{z}$. For the length scales of interest to us (see appendix A for a more detailed discussion) the lattice system can be coarse-grained so that the magnetic state of the system is described by a magnetization $\boldsymbol{M}(\boldsymbol{x}, t)$ defined on a 3D spatial continuum. The total static energy in the absence of an external magnetic field is the sum of the exchange, anisotropy and demagnetization energies. A stationary Bloch wall is a soliton configuration of the magnetization $\boldsymbol{M}(\boldsymbol{x})$ with vanishing demagnetization energy, subject to the boundary condition $\boldsymbol{M}(y \to \pm\infty) = \pm M\hat{z}$ (see figure 1). The spatial variation of the wall is localized to a planar (flat) region of thickness $\lambda = \sqrt{J/K}$ (J = exchange stiffness constant) which is assumed to be parallel to the xz-plane. The wall coordinate q specifies the distance from the origin to a reference point on the wall ($\boldsymbol{x}_{\text{wall}} = q\hat{y}$) [15].

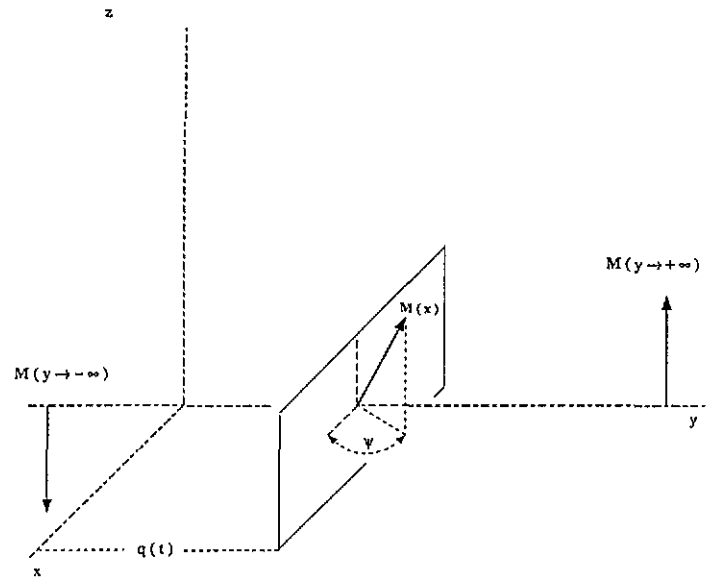

Figure 1. A Bloch wall located at $\boldsymbol{x}_{\text{wall}} = q\hat{y}$.

Voids in the magnetic insulator act as pinning sites for the wall. For insulators with $Q \gg 1$, the attraction is due primarily to a reduction in the exchange and anisotropy energies which occurs when the wall sits on the void. For a void of length scale R satisfying $l_0 \ll R \ll \lambda$ (l_0 = lattice constant $\equiv 5$ Å), located at the origin, the pinning potential seen by a flat Bloch wall is $U(q) = -U_0 \operatorname{sech}^2(q/\lambda)$ (see appendix B), where $U_0 = 2KV_d$ and V_d is the void volume. In our calculation, $\lambda = 1000$ Å (50 Å) for walls with $N \geqslant 10^4$

($300 \leqslant N \leqslant 3000$) and $U_0 = 0.1$ eV (1.0×10^{-5} eV). For LaGaYIG, $Q = 25.2$ and $K \simeq 2000\,\mathrm{erg\ cm^{-3}}$, so that for a spherical void $R \simeq 200$ Å (10 Å). We consider two spherical voids located at $x_\pm = \pm Q_0\hat{y}$ ($L = 2Q_0$) with volumes $V_+ = aV_-$ ($a \geqslant 1$). They produce the double-well pinning potential

$$U(q) = -U_0\left[\operatorname{sech}^2\left(\frac{q+Q_0}{\lambda}\right) + a\operatorname{sech}^2\left(\frac{q-Q_0}{\lambda}\right)\right].$$

When $a = 1$ we obtain a symmetric double-well potential (SDWP); otherwise, the wall sees an asymmetric double-well potential (AsDWP). For an energy E corresponding to QC there will be four turning points $T_1 < T_2 < T_3 < T_4$. We refer to the region $q < T_1$ as the 'left barrier', the region $T_1 < q < T_2$ as the 'left well', the region $T_2 < q < T_3$ as the 'central barrier', the region $T_3 < q < T_4$ as the 'right well', and the region $T_4 < q$ as the 'right barrier'. Varying the void separation L (i.e. Q_0) varies the depth of the wells and the height and width of the central barrier. It is important to realize that the well minima do *not* occur at $q = \pm Q_0/2$ unless $L \gg \lambda$. In fact, the central barrier disappears completely for $L \approx 1.3\lambda$. This can be understood as a simple consequnce of the finite thickness of the wall. When $L \approx 1.3\lambda$, the voids are so close together that the wall can straddle both voids simultaneously so that there is no barrier for the wall to move from one void to the other. The experimental situation envisioned is either (1) a thin film or (2) a very narrow wire of the magnetic insulator in which only one Bloch wall is present [8]. In the thin-film case, only a small region (of the wall) of cross-sectional area A_w is involved in tunnelling between the pinning sites [8]. In our analysis below, we treat the wall as if it were flat, whereas, for the thin-film scenario, it will in fact be curved in the vicinity of the void. Curvature effects will be discussed in section 5. In the case of the very thin wire, curvature effects are not expected to be important because of the large energy required to bend the wall on a length scale of the order of the cross-sectional dimension of the wire.

A flat Bloch wall can be made to move by applying a torque along the easy axis of the material. For our situation this can be accomplished by inducing magnetic poles on the surface of the wall. This leads to an increase in the total energy of the wall due to the demagnetization energy produced by the surface poles interacting with the Bloch wall magnetization. This increase in wall energy is interpreted as wall kinetic energy which allows a definition of the wall (Döring) mass M_D [15]

$$M_D = \frac{A_w}{2\pi\gamma^2\lambda}. \tag{1}$$

Here A_w is the area of the moving section of the wall, and γ is the gyromagnetic ratio. We thus arrive at our wall Hamiltonian $H = p^2/2M_D + U(q)$. Introducing the dimensionless length $x = q/\lambda$ and the energy scale $\mathcal{S} = \hbar^2/2M_D\lambda^2$, we can write the time-independent Schrödinger equation in the dimensionless form

$$\left[\frac{\mathrm{d}^2}{\mathrm{d}x^2} + \mathcal{U}_0\left\{\operatorname{sech}^2(x+x_0) + a\operatorname{sech}^2(x-x_0)\right\} + \mathcal{E}\right]\psi = 0.$$

Here $\mathcal{U}_0 = U_0/\mathcal{S}$, $x_0 = Q_0/\lambda$ and $\mathcal{E} = E/\mathcal{S}$. The dimensionless potential strength $\mathcal{U}_0$ is related to the wall size $N = A_w\lambda/l_0^3$ by

$$\mathcal{U}_0 = \left(\frac{U_0 l_0^3}{\pi^2 g^2 \mu_B^2}\right) N$$

where g is the electron g-factor, and μ_B is the Bohr magneton.

3. The numerical calculation

We begin with the calculation of E_0, E_1 and ψ_0, ψ_1 for the SDWP ($a = 1$). In this case, the wavefunctions have definite parity and we can restrict our attention to $x_1 \leqslant x \leqslant x_2 = 0$. The boundary condition on ψ_0 at x_2 is that its slope vanishes, while for ψ_1, that it has a node at $x_2 = 0$. The boundary condition at x_1 is that the WKB approximation applies at x_1. This is always possible for x_1 sufficiently far inside the left barrier. Thus x_1 is chosen so that

$$\frac{M_D\hbar}{p^3(x)}\left|\frac{dU}{dx}\right|_{x_1} \ll 1 \tag{2}$$

which requires an initial guess for the energy E. To obtain this initial guess, we locate the minimum x_{min} of the left well numerically for a given x_0 and then approximate the SDWP near x_{min} by an equivalent harmonic oscillator potential. The ground-state and first-excited-state energies of the oscillator provide our initial guesses for E_0, E_1.

We utilize a shooting algorithm [18] to solve the eigenvalue problem numerically. This algorithm takes initial values for ψ, $d\psi/dx$ at the boundaries x_1 and x_2, consistent with the boundary conditions, and uses the Schrödinger equation to continue these boundary values to an interior point x_f ($x_1 < x_f < x_2$). We will refer to the continuation from x_1 to x_f as the 'left shot', and that from x_2 to x_f as the 'right shot'. Unfortunately, the wavefunctions cannot be solved for directly because for walls as large as are of interest to us, $\mathcal{U}_0$ is enormous ($10^2 < \mathcal{U}_0 \leqslant 10^{11}$). As the wavefunctions depend exponentially on $\mathcal{U}_0$ inside the barriers, the numerical problem is unstable. For the ground state we introduce an auxiliary function $g_0(x)$

$$\psi_0(x) \equiv \exp[g_0(x)]. \tag{3}$$

This transformation is well defined for the ground state since $\psi_0(x) \neq 0$ for $x_1 \leqslant x \leqslant x_2$. Inserting (3) into the Schrödinger equation gives

$$\frac{d^2g_0}{dx^2} + \left(\frac{dg_0}{dx}\right)^2 + \mathcal{E} + \mathcal{U}_0\left[\operatorname{sech}^2(x + x_0) + \operatorname{sech}^2(x - x_0)\right] = 0. \tag{4}$$

The shooting algorithm can be applied to (4), where $g_0(x_1)$ and $dg_0(x_1)/dx$ are equal to the WKB exponent and its derivative at x_1. At x_2, we guess initially $g_0(x_2)$ by approximating $\psi_0(x)$ via WKB at the origin. The boundary condition on $d\psi_0(x_2)/dx$ requires $dg_0(x_2)/dx \equiv 0$. The algorithm improves the initial guesses for E_0 and $g_0(x_2)$ iteratively, and iteration ceases when the most recent correction ΔE to the most recent energy E satisfies $\Delta E < 10^{-14}E$. Since the first-excited-state wavefunction has a node at x_2, the transformation (3) is useless there. Instead, we define $\psi_1(x) = \sinh[g_R(x)]$ for the right shot and $\psi_1(x) = \exp[g_L(x)]$ for the left shot. $g_R(x)$ satisfies

$$\frac{d^2g_R}{dx^2} + \tanh(g_R)\left[\left(\frac{dg_R}{dx}\right)^2 + \mathcal{E} + \mathcal{U}_0\left\{\operatorname{sech}^2(x + x_0) + \operatorname{sech}^2(x - x_0)\right\}\right] = 0. \tag{5}$$

The boundary condition at x_2 is $g_R(x_2) = 0$ and $dg_R(x_2)/dx$ is guessed by approximating $\psi_1(x_2)$ via WKB near the origin. The left shot for g_L goes through exactly as for g_0. The algorithm improves the initial guesses for E_1 and $dg_R(x_2)/dx$ iteratively to the same precision as for the ground state.

For the AsDWP, the wavefunctions are no longer parity eigenstates. The boundary points are now $x_{1R} = -x_{1L} > 0$. Numerical stability requires two fitting points x_{fL}, x_{fR} inside the left and right wells respectively. As before $x_2 = 0$. The 'left shot' proceeds from x_{1L} to

x_{fL}, and the 'right shot' from x_{1R} to x_{fR}. Two shots originate from x_2: one to x_{fL} and the other to x_{fR}. As with the SDWP calculation, x_{1L} (x_{1R}) is chosen sufficiently far inside the left (right) barrier so that the WKB approximation applies there. The boundary conditions at x_{1L}, x_{1R} are specified as in the SDWP calculation, only now the initial guesses for $g_0(x_{1R})$ and $g_1(x_{1R})$ are improved iteratively ($g_0(x_{1L})$, $g_1(x_{1L})$ amount to choices of normalization and require no improvements). The algorithm iterates and terminates under the same conditions as in the SDWP calculation.

4. Results and analysis

Our results for the tunnelling gap Δ_0 appear in tables 1 and 2 and correspond to macroscopic and mesoscopic walls of thickness $\lambda = 1000$ Å and 50 Å respectively. So far we have assumed our system of wall and voids to be completely isolated. If a weak stray magnetic field $\boldsymbol{H}_{ext}$ were present, it would produce a bias ϵ in the gap $\Delta = \sqrt{\Delta_0^2 + \epsilon^2}$. This bias is a consequence of the Zeeman energy density $-\boldsymbol{M} \cdot \boldsymbol{H}_{ext}$. For an actual stray field, the direction of $\boldsymbol{H}_{ext}$ is unknown and the experimentally relevant bias $\bar{\epsilon}$ is obtained by averaging over this direction. It is easily shown that $\bar{\epsilon} \simeq MA_wLH_{ext}$. We take $H_{ext} \simeq 10^{-6}$ G as indicative of the magnitude of a stray magnetic field (AC magnetic fields of 10^{-5} G have been used in measurements of the frequency-dependent magnetic susceptibility [6]). Clearly, a necessary condition for observable domain wall QC is $\Delta_0 > \bar{\epsilon}$. For $N \geqslant 10^4$, we find that $A_w = (1.1 \times 10^{-17}\ \text{cm}^2)N$ (and $M_D = (5.6 \times 10^{-28}\ \text{g})N$), so that for LaGaYIG for which $M \simeq 10$ G, $\bar{\epsilon} = (1.04 \times 10^{-11}\ \text{K})N$. Thus the bias grows with wall size N, making observation of QC more difficult for the larger walls. To proceed further, note that there exists a limited range of void separations for which Δ_0 corresponds to QC *and* still satisfies $\Delta_0 > \bar{\epsilon}$. For $L < L_{min}$, the ground-state energy is above the central barrier, while if $L > L_{max}$, $\Delta_0 < \bar{\epsilon}$. Let $\mathcal{R} = L_{max} - L_{min}$ be the size of the allowed range of void separations. Its value is given in table 1 and is obtained (for a given N) by comparing Δ_0 and L with $\bar{\epsilon}$. Quantum coherence will be observable only when (i) the uncertainty in L satisfies $\Delta L \ll \mathcal{R}$ and (ii) $\mathcal{R} \gg \mathcal{C}$, where $\mathcal{C} \simeq (2\text{–}3)l_0$ is the coarse-graining length scale. One expects that $\Delta L \simeq l_0$ and in our calculation $l_0 = 5$ Å. If either (or both) of these conditions is (are) not satisfied one would expect that the experimentally relevant gap would be an average of Δ_0 over the appropriate length scale. From table 1 we see that, for $N \geqslant 10^4$, such an average is necessary and that any reasonable procedure gives $\bar{\Delta} < \bar{\epsilon}$. Thus macroscopic QC ($N \geqslant 10^4$) is not expected to be observable due to the rapid variation of the tunnelling gap with small changes in L and the large bias $\bar{\epsilon}$ introduced by a stray magnetic field. We also see that in the case of the SDWP (in the absence of dissipation), the conditions for observable QC do not rule out walls with $N \simeq 10^2$–10^3 (see table 2) which would correspond to mesoscopic quantum coherence. (Here $A_w = (2.67 \times 10^{-16}\ \text{cm}^2)N$, $M_D = (2.73 \times 10^{-25}\text{g})N$ and $\bar{\epsilon}$ is given in table 2.) We now go on to examine the effects of void asymmetry on the case of mesoscopic QC.

Since $U_0 = 2KV_d$, the larger the void, the more strongly it attracts the wall. Thus, if void asymmetry is sufficiently pronounced, QC is lost because the larger void pins the wall. This effect can be seen by following the ground-state energy as we increase a from unity (see table 3). Imagine $a = 1$ (corresponding to a SDWP) and that $\{N, U_0, L\}$ are such that, in the absence of dissipation, we have QC. Imagine further that we increase a so that the void at $q = Q_0$ attracts the wall more strongly than the other void. This stronger attraction causes E_0 to decrease (i. e. become more negative) as the probability distribution in the ground state begins to shift towards $q = Q_0$. As we continue to increase a, we reach a critical

Table 1. Tunnelling gap Δ_0; width $\mathcal{R}$ of range of observable void separations; central barrier height U_{bh}; and bias $\bar{\epsilon}$ for a macroscopic Bloch wall moving in an SDWP.

N (spins)	L (Å)	Δ_0 (K)	$\mathcal{R}$ (Å)	U_{bh} (K)	$\bar{\epsilon}$ (K)
10^4	1320	AB[a]	$\simeq 6$	—	1.04×10^{-7}
	1322	4.0×10^{-4}		1.8×10^{-2}	
	1324	2.0×10^{-5}		3.6×10^{-2}	
	1326	5.0×10^{-7}		5.9×10^{-2}	
10^5	1318	AB	$\simeq 2$	—	1.04×10^{-6}
	1319	1.8×10^{-4}		3.0×10^{-3}	
	1320	9.6×10^{-6}		6.7×10^{-3}	
	1321	2.0×10^{-7}		1.2×10^{-2}	
10^6	1317	AB	$\simeq 1$	—	1.04×10^{-5}
	1318	2.4×10^{-5}		7.9×10^{-4}	
	1319	9.1×10^{-9}		3.0×10^{-3}	
	1320	$< 7.2 \times 10^{-11}$		6.7×10^{-3}	
10^7	1317.2	AB	< 0.1	—	1.04×10^{-4}
	1317.3	2.0×10^{-5}		8.5×10^{-5}	
	1317.4	8.2×10^{-6}		1.4×10^{-4}	
	1317.6	4.0×10^{-7}		3.0×10^{-4}	
	1318.0	2.2×10^{-10}		7.9×10^{-4}	

[a] AB = ground state above barrier.

Table 2. Tunnelling gap Δ_0; width $\mathcal{R}$ of range of observable void separations; central barrier height U_{bh}; and bias $\bar{\epsilon}$ for a mesoscopic Bloch wall moving in an SDWP.

N (spins)	L (Å)	Δ_0 (K)	$\mathcal{R}$ (Å)	U_{bh} (K)	$\bar{\epsilon}$ (K)
300	74	AB[a]	$\simeq 30$	—	5.2×10^{-9}
	75	1.1×10^{-3}		3.3×10^{-3}	
	80	2.5×10^{-4}		7.2×10^{-3}	
	103	7.7×10^{-9}		3.2×10^{-2}	
	110	2.4×10^{-10}		4.0×10^{-2}	
	120	1.8×10^{-12}		5.2×10^{-2}	
3000	69	AB	$\simeq 10$	—	4.3×10^{-8}
	75	3.1×10^{-6}		3.3×10^{-3}	
	80	6.1×10^{-9}		7.2×10^{-3}	

[a] AB = ground state above barrier.

value a_* at which E_0 is equal to the value of the AsDWP at the metastable minimum of the left well U_{meta}. For $a > a_*$, E_0 drops below the metastable minimum which corresponds to the pinning of the wall at $q = Q_0$ and the destruction of QC. Intuitively, we expect that when $\Delta U_0 = U_0^+ - U_0^- = (a-1)U_0^-$ is approximately equal to the barrier height U_{bh} of the SDWP, the larger void will pin the wall. For mesoscopic walls, U_{bh} is given in table 2. For $N = 300$, $L = 75$ Å; $U_{bh} = 2.8 \times 10^{-7}$ eV (note the difference in units relative to table 2). Thus $\Delta U_0 = U_{bh}$ corresponds to $\overline{a_*} \approx 1.008$. A numerical calculation of E_0 for this case gives $a_* = 1.038 > \overline{a_*}$ (see table 3). For the spherical voids we have been considering, if $R_- = 10$ Å, then $R_+ = a_*^{1/3} R_- = 10.1$ Å. Thus if asymmetry is not to destroy QC, the radii of the two voids must satisfy $\Delta R = R_+ - R_- < 0.1$ Å. Such a tolerance is clearly unattainable and since $\Delta R \ll C$ we must average the effects of asymmetry over the coarse-graining length scale $C \simeq 10$–15 Å. As the majority of ΔR values entering into the average correspond to pinning of the wall, we conclude that asymmetry in the voids acts to

destroy QC in this case. We might hope to overcome this difficulty by increasing L and so increasing U_{bh}. For $L = 103$ Å, $N = 300$, the SDWP tunnelling gap is $\Delta_0 = 7.7 \times 10^{-9}$ K (see table 2). At this separation, QC is marginally observable in the absence of dissipation. In this case $U_{bh} = 2.8 \times 10^{-6}$ eV (see table 2). Then $\Delta U_0 = U_{bh}$ gives $\overline{a_*} = 1.085$. We did not determine a_* numerically for this case. In the previous example we saw that $(a_* - 1) \simeq 5(\overline{a_*} - 1)$ so we will estimate $(a_* - 1) \simeq 10(\overline{a_*} - 1)$ for this case. This gives $a_* \simeq 1.85$. For $R_- = 10$ Å, $\Delta R \simeq 2.3$ Å. Again $\Delta R < C$ so that an average of the effects of asymmetry over $C \simeq 10$–15 Å is necessary. As in the previous case, the majority of the ΔR values correspond to pinning of the wall so that we again conclude that asymmetry in the voids will act to destroy QC in this already marginal case. Larger values of L lead to $\Delta_0 < \bar{\epsilon}$. We see that asymmetry of the voids will be sufficient to destroy any remaining vestige of domain wall QC—even in the *absence of dissipation*. The basic difficulty is that maximizing the tunnelling gap requires a very small central barrier: so small, in fact, that the most minute asymmetry in the two voids produces a bias in the double well which is of order of the height of the central barrier and so capable of pinning the wall (i.e. destroying QC). We suspect that this is generally true of macroscopic QC: large objects require small barriers which are easily removed by small imperfections in the experimental set-up.

Table 3. Asymmetry parameter a; ground-state energy E_0; metastable minimum U_{meta} of ASDWP; and barrier height U_{bh} for a mesoscopic Bloch wall with $N = 300$ and void separation $L = 75$ Å.

a	E_0 (K)	U_{meta} (K)	U_{bh} (K)
1.000	-1.4638×10^{-1}	-1.4859×10^{-1}	3.33×10^{-3}
1.010	-1.4719×10^{-1}	-1.4894×10^{-1}	2.96×10^{-3}
1.020	-1.4814×10^{-1}	-1.4930×10^{-1}	2.59×10^{-3}
1.030	-1.4914×10^{-1}	-1.4966×10^{-1}	2.23×10^{-3}
1.038	-1.4997×10^{-1}	-1.4995×10^{-1}	1.94×10^{-3}

5. Summary and closing remarks

In this paper we have carried out a numerical analysis of domain wall quantum coherence in a uniaxial magnetic insulator with quality factor $Q \gg 1$ at $T = 0$. We find that QC on any scale larger than microscopic appears unlikely due to the combined effects of stray magnetic fields and asymmetry in the voids which are responsible for producing the double-well potential seen by the domain wall. Our calculation assumed a flat wall although curved walls are expected in the vicinity of the voids in the thin-film scenario. For this scenario, and for voids of given size, tunnelling will only occur if $L < L_{crit}$ when curvature effects are included [8]. This is because the curvature energy acts to raise the minima of the DWP relative to the top of the central barrier, thus reducing U_{bh}. When $L = L_{crit}$, the central barrier has disappeared and we are no longer in the QC regime. If $L_{crit} > L_{max}$, the tunnelling gap becomes unobservable before curvature effects become significant. Otherwise, $L_{crit} < L_{max}$ and curvature effects act to reduce the range of void separation $\mathcal{R} \to \mathcal{R}_{new} = L_{crit} - L_{min}$ corresponding to QC. For macro-walls, $\mathcal{R}$ was already small enough to rule out macro-QC so that decreasing $\mathcal{R} \to \mathcal{R}_{new}$ acts to strengthen this conclusion. For meso-walls, if $\mathcal{R}_{new} < C$, then curvature effects have reduced the range of QC sufficiently that stray magnetic fields are expected to make meso-QC unobservable. Finally, if $\mathcal{R}_{new} > C$, asymmetry in the void sizes can more easily destroy meso-QC since

curvature effects act to reduce U_{bh}. Thus curvature effects are not expected to modify our conclusion that observation of meso- or macro-QC of domain walls appears unlikely. It should be noted that the phase coherences necessary for establishing quantum coherence are much more delicate than those necessary for establishing quantum tunnelling so that our work does not preclude *a priori* the possibility of observing macroscopic quantum tunnelling of domain walls in magnetic insulators.

Acknowledgments

I would like to thank Philip Stamp for useful discussions, Anupam Garg for stressing the importance of void asymmetry, T Howell III for support and NSERC of Canada for financial support.

Appendix A. Influence of a void on Bloch wall structure

The aim of this appendix is to introduce a calculational scheme allowing us to determine iteratively the modification of the 180° Bloch wall structure caused by a void in a high-quality $Q = K/2\pi M^2 \gg 1$ (where K is the anisotropy constant and M is the spontaneous magnetization) magnetic insulator in which the wall is present. We will see that for a sufficiently small void (see below) in such a material, the Bloch wall structure is not significantly modified outside the void.

The system of interest is a lattice of spins (with lattice constant l_0) coupled to each other via the exchange and dipole–dipole interactions; and to the underlying lattice via the magnetic anisotropy interaction which is assumed to be uniaxial with easy axis along $\hat{z}$. For the length scales of interest to us the lattice system can be coarse-grained so that the magnetic state of the system is described by a magnetization $M(x, t)$ defined on a 3D spatial continuum. The total static energy for this system is given by

$$E = \int_V d^3x \left[J(\partial_i \hat{M}_j)^2 + K(\hat{M}_x^2 + \hat{M}_y^2) - \frac{1}{2} M \cdot H_d \right] \tag{A1}$$

where

$$H_d(x) = -\nabla_x \left[\oint_S \frac{\hat{n}' \cdot M(x')\, da'}{|x - x'|} - \int_V \frac{\nabla \cdot M(x')\, d^3x'}{|x - x'|} \right]. \tag{A2}$$

Here J is the exchange stiffness constant, K is the anisotropy constant, V is the volume occupied by the magnetic system and $S = \partial V$ is the boundary of V with outward normal $\hat{n}'$; and repeated indices are summed over. H_d is the demagnetization field produced by $M(x, t)$ and the last term in (A1), referred to as the demagnetization energy, is a consequence of the dipole–dipole interaction.

The flat Bloch wall is a static, smoothly varying configuration of $M(x)$ that interpolates between two regions (domains) of uniform (and distinct) magnetization. A 180° Bloch wall (to which we restrict ourselves) is an extremum of the total static energy (A1) with vanishing demagnetization energy satisfying the boundary conditions

$$M(y \to \pm\infty) = \pm M\hat{z}. \tag{A3}$$

We further restrict ourselves to high-quality ($Q \equiv K/2\pi M^2 \gg 1$) magnetic insulators so that the low-energy wall dynamics is describable in terms of a moving flat Bloch wall with

wall coordinate $q(t) = q(t)\hat{y}$ and angle ψ giving the azimuthal angle in the xy-plane of M [15]. For an infinite medium, the Bloch wall magnetization is [1]

$$M_w(x,t) = M \begin{pmatrix} (1-\dot{q}^2/8c_0^2)\ \text{sech}\,([y-q(t)]/\lambda) \\ (\dot{q}/8c_0)\ \text{sech}\,([y-q(t)]/\lambda) \\ \tanh\,([y-q(t)]/\lambda) \end{pmatrix}. \tag{A4}$$

Here $\lambda = \sqrt{J/K}$ is the Bloch wall thickness, $c_0 = 2\pi\gamma\lambda M \simeq 10^2$ cm s^{-1} is the Walker velocity (γ is the gyromagnetic ratio), and $\dot{q} < c_0$. It is clear from (A4) that a static Bloch wall has $H_d = 0$.

Imagine introducing a void of volume V_d into a high-Q magnetic insulator such as LaGaYIG. This will modify the magnetization $M(x)$ outside the void because a distribution of magnetic 'charge' ($\sigma = M \cdot \hat{n}$) is induced on the surface of the void S_d. This induced magnetic charge produces a demagnetization field outside the void which is responsible for the modification $M_1(x)$ in the Bloch wall magnetization $M_w(x)$,

$$M(x) = M_w(x) + M_1(x). \tag{A5}$$

Since $Q \gg 1$, the exchange and magnetic anisotropy energies dominate the demagnetization energy so that one expects that if the void is not too large, $|M_1(x)| \ll |M_w(x)|$. If R is the length scale of the void and λ is the wall thickness, we expect that when $R \ll \lambda$, $|M_1(x)| \ll |M_w(x)|$. We will say that the void is 'sufficiently small' when this condition is satisfied. Note that $R \gg l_0$, where l_0 is the lattice constant, if the coarse-graining approximation is to be meaningful. We also assume a smooth void surface so that singularities in the induced magnetic surface charge will not occur. We thus assume the following conditions to be satisfied: (i) $Q \gg 1$; (ii) $l_0 \ll R \ll \lambda$; and (iii) the void surface S_d is smooth.

Although the void is not expected to be spherical in general, we will make the approximation that the actual void can be replaced by a spherical void of radius $R_0 \ll \lambda$ such that $\Delta V = V_d - V_{sph} \ll V_d$, where $V_{sph} = 4\pi R_0^3/3$. Corrections to our spherical approximation will arise from (i) the regions of V_d that lie outside V_{sph} and (ii) the regions of V_{sph} that lie outside V_d. We will see at the end of this appendix that such corrections are negligible when $\Delta V \ll V_d$.

When $Q \gg 1$, the dynamical wall structure is due primarily to the exchange and magnetic anisotropy energies. Dynamic reaction forces and magnetostatic forces lead to small perturbations in the structures determined by exchange and anisotropy [15]. A Bloch wall whose normal lies along the y-axis (with easy axis along the z-axis) and whose magnetization is specified by the angles ($\theta = \theta(y)$, $\phi = \phi(y)$) via $M(x) = M(\sin\theta\cos\phi, \sin\theta\sin\phi, \cos\theta)$, has a total static energy density w given by

$$w = w_{ex} + w_{anis} + \mathcal{O}(Q^{-1}) = J\left[\left(\frac{\partial\theta}{\partial y}\right)^2 + \left(\sin\theta\frac{\partial\phi}{\partial y}\right)^2\right] + K\sin^2\theta + \mathcal{O}(Q^{-1}). \tag{A6}$$

Requiring that the total static energy $E = \int d^3x\, w(x)$ be stationary against small variations leads to the Euler–Lagrange equations

$$J\left[\sin^2\theta\frac{\partial^2\phi}{\partial y^2} + \sin\ 2\theta\left(\frac{\partial\phi}{\partial y}\right)\left(\frac{\partial\theta}{\partial y}\right)\right] = 0 \tag{A7}$$

$$2J\frac{\partial^2\theta}{\partial y^2} - \left(K + J\left(\frac{\partial\phi}{\partial y}\right)^2\right)\sin\ 2\theta = 0. \tag{A8}$$

The Bloch wall configuration (θ_w, ϕ_w) given in (A4) corresponds to the solution of (A8) satisfying the boundary conditions

$$\theta(y) \to \begin{cases} \pi & y \to -\infty \\ 0 & y \to +\infty. \end{cases} \tag{A9}$$

Introducing a spherical void of radius R_0 at the origin leads to modification of the Euler–Lagrange equations which must be solved to obtain the modified Bloch wall structure. As $R_0 \ll \lambda$, we require θ, ϕ to be constant on S_d (i.e. M does not vary on S_d). Our remaining boundary condition is that $M(x) \to M_w(x)$ as $|x| \to \infty$.

We determine $M(x)$ iteratively. We assume $(\theta^{(0)}, \phi^{(0)}) = (\theta_w, \phi_w)$ outside the void (i.e. $M^{(0)} = M_w$ outside the void). This leads to induced magnetic charges on S_d as described above that produce a demagnetization field H_d. This field interacts with the modified magnetization $M^{(1)} = M^{(0)} + \delta M^{(0)} \equiv M\hat{m}^{(1)}$ via the demagnetization energy whose density is $w_{demag} = -M^{(1)} \cdot H_d/2$. The strategy is to obtain new Euler–Lagrange equations whose solution

$$\begin{aligned} \theta^{(1)}(\rho, y) &= \theta^{(0)}(y) + \delta\theta^{(0)}(\rho, y) = \theta_w(y) + \delta\theta^{(0)}(\rho; y) \\ \phi^{(1)}(\rho, y) &= \phi^{(0)}(y) + \delta\phi^{(0)}(\rho, y) = \phi_w(y) + \delta\phi^{(0)}(\rho, y) \end{aligned} \tag{A10}$$

will determine the lowest-order correction to the Bloch wall structure. In (A10) we have adopted cylindrical coordinates (ρ, α, y), where (ρ, α) are polar coordinates for the xz-plane. As $\theta^{(1)}, \phi^{(1)}$ now depend on ρ, the exchange energy density is modified to

$$w_{exc} \to \bar{w}_{exc} = J\left[\left(\frac{\partial\theta^{(1)}}{\partial\rho}\right)^2 + \left(\frac{\partial\theta^{(1)}}{\partial y}\right)^2 + \sin^2\theta^{(1)}\left\{\left(\frac{\partial\phi^{(1)}}{\partial\rho}\right)^2 + \left(\frac{\partial\phi^{(1)}}{\partial y}\right)^2\right\}\right]. \tag{A11}$$

The total static energy density in the presence of the spherical void becomes

$$w = \bar{w}_{exc} + w_{anis} + w_{demag}. \tag{A12}$$

In appendix B we show that when $M = M^{(0)}$, the demagnetization field H_d corresponds to a dipole field

$$H_d(x) = \frac{MV_d}{r^3}\left[\hat{m} - 3\hat{x}(\hat{m} \cdot \hat{x})\right] \equiv \frac{MV_d}{r^3} d(x) \tag{A13}$$

where $\hat{m} \equiv M^{(0)}(0)/M$. This gives a demagnetization energy density

$$w_{demag} = -\frac{M^2V_d}{2r^3}\hat{m}^{(1)} \cdot d = -\frac{M^2V_d}{2r^3} f(\theta^{(1)}, \phi^{(1)}; d) = -KQ^{-1}\frac{V_d}{4\pi r^3} f(\theta^{(1)}, \phi^{(1)}; d). \tag{A14}$$

The new Euler–Lagrange equations arising from (A12) are

$$J\left[\sin^2\theta^{(1)}\left(\frac{\partial^2\phi^{(1)}}{\partial\rho^2} + \frac{\partial^2\phi^{(1)}}{\partial y^2}\right) + \sin 2\theta^{(1)}\left\{\left(\frac{\partial\phi^{(1)}}{\partial y}\right)\left(\frac{\partial\theta^{(1)}}{\partial y}\right) + \left(\frac{\partial\phi^{(1)}}{\partial\rho}\right)\left(\frac{\partial\theta^{(1)}}{\partial\rho}\right)\right\}\right] = KQ^{-1}\frac{V_d}{4\pi r^3}\frac{\partial f}{\partial\phi^{(1)}} \tag{A15}$$

$$2J\left[\frac{\partial^2\theta^{(1)}}{\partial y^2} + \frac{\partial^2\theta^{(1)}}{\partial\rho^2}\right] - \left[K + J\left\{\left(\frac{\partial\phi^{(1)}}{\partial y}\right)^2 + \left(\frac{\partial\phi^{(1)}}{\partial\rho}\right)^2\right\}\right]\sin 2\theta^{(1)} = KQ^{-1}\frac{V_d}{4\pi r^3}\frac{\partial f}{\partial\theta^{(1)}}.$$

Inserting (A10) into (A16) and keeping terms only to first order in small quantities gives (recall $J = K\lambda^2$)

$$\lambda^2 \sin^2\theta_w \frac{\partial^2(\delta\phi^{(0)})}{\partial\rho^2} = Q^{-1}\frac{V_d}{4\pi r^3}\left.\frac{\partial f}{\partial\phi}\right|_{(\theta_w,\phi_w)}$$
$$2\lambda^2\frac{\partial^2(\delta\theta^{(0)})}{\partial\rho^2} = Q^{-1}\frac{V_d}{4\pi r^3}\left.\frac{\partial f}{\partial\theta}\right|_{(\theta_w,\phi_w)}. \tag{A16}$$

As expected, the 'source terms' on the RHS of (A16) vanish as $V_d \to 0$ so that $M \to M_w$ in this limit. Also, since $Q^{-1} \ll 1$, the source terms are small so that $\delta\theta^{(0)}$ and $\delta\phi^{(0)}$ will be small.

Assuming we have obtained solutions to (A16), we proceed iteratively. Our initial guess $\theta^{(0)} = \theta_w$, $\phi^{(0)} = \phi_w$ has now been corrected to $\theta^{(1)} = \theta_w + \delta\theta^{(0)}$, $\phi^{(1)} = \phi_w + \delta\phi^{(0)}$. This yields an improved magnetization $M^{(1)} = M_w + \delta M^{(0)}$. We then use $M^{(1)}$ to obtain the corrections to the demagnetization energy which then modify the Euler–Lagrange equations. Writing $\theta^{(2)} = \theta^{(1)} + \delta\theta^{(1)}$; $\phi^{(2)} = \phi^{(1)} + \delta\phi^{(1)}$ we solve the new Euler–Lagrange equations for $\delta\theta^{(1)}$, $\delta\phi^{(1)}$. Having done so, one can repeat the procedure until the physically relevant degree of accuracy is achieved.

The above calculation assumed a spherical void. For a non-spherical void, we assume S_d is sufficiently well behaved so that we can find a 'best' sphere of radius R_0 such that $0 < V_d - 4\pi R_0^3/3 \ll V_d$. We have seen that the spherical void produces a demagnetization field that is dipolar in character. It is clear that corrections to this dipole field will come from (i) the region of V_d lying outside the 'best' sphere and (ii) the region of the 'best' sphere lying outside V_d, and that these regions will lead to higher multipole moment corrections to the dipole field. It is also clear that the relative strength of the contribution to H_d from a multipole moment of order l to the dipole contribution will be of order

$$\frac{V_d - V_{sph}}{V_d}\left(\frac{R_0}{r}\right)^{l-3} \qquad (l \geqslant 4) \tag{A17}$$

which is manifestly negligible outside the void when $V_d - V_{sph} \ll V_d$. In such cases it should be adequate to approximate the void by the 'best' spherical void.

Thus for the type of voids to which we have restricted ourselves in this paper ($Q^{-1} \ll 1$; $l_0 \ll R_0 \ll \lambda$; smooth void surface), we see that corrections to the Bloch wall structure (A4) produced by the presence of the void will be small. Thus we make the approximation $M(x) = M_w(x)$ (outside the void) in our calculation of the pinning potential given in appendix B.

Appendix B. Calculation of the pinning potential

In this appendix we will calculate the pinning potential acting on a Bloch wall at $q\hat{y}$ due to a spherical void of radius R_0 centred on the origin. Our result $U(q) = -U_0\,\mathrm{sech}^2(q/\lambda)$, where λ is the wall thickness, reproduces the functional form of the pinning potential obtained by Stamp [7], although we obtain a different result for the potential strength U_0. The pinning potential is the difference in the total static energy of the wall for the two cases in which the void is and is not present. We assume $l_0 \ll R_0 \ll \lambda$ (see appendix A) and that the wall plane is parallel to the xz plane. We further assume that the Bloch wall is present in a high-quality ($Q \gg 1$) magnetic insulator so that, as seen in appendix A, the magnetization

outside the void does not significantly deviate from the Bloch wall form. Thus we take

$$M(x) = \begin{cases} 0 & |x| < R_0 \\ M_w(x) & |x| \geqslant R_0 \end{cases} \tag{B1}$$

and $M_w(x)$ is the Bloch wall magnetization (A4) of a wall at $q\hat{y}$. For convenience, we assume $\dot{q} = 0$. The pinning potential receives contributions from the exchange, magnetic anisotropy, and demagnetization energies

$$U(q) = U_{exc}(q) + U_{anis}(q) + U_{demag}(q). \tag{B2}$$

We begin with the exchange contribution to $U(q)$. Let $R^3 - V_d$ denote the region outside the void. Then

$$U_{exc}(q) = \left[\int_R^3 - V_d - \int_R^3\right] d^3x \; J\left(\partial_i \hat{m}_j\right)\left(\partial_i \hat{m}_j\right) \tag{B3}$$

and $\hat{m} = M_w/M$. Simple algebra gives

$$U_{exc}(q) = -\int_{V_d} d^3x \, \frac{J}{\lambda^2} \operatorname{sech}^2\left(\frac{y-q}{\lambda}\right) = -K\int_{V_d} d^3x \left[\frac{\operatorname{sech}(y/\lambda)\operatorname{sech}(q/\lambda)}{1-\tanh(y/\lambda)\tanh(q/\lambda)}\right]^2. \tag{B4}$$

For a Bloch wall, $J = K\lambda^2$ has been used and since $|x| \leqslant R_0 \ll \lambda$, we can expand the hyperbolic functions to lowest order in y/λ

$$\begin{aligned} U_{exc}(q) &= -K\operatorname{sech}^2(q/\lambda)\int_{V_d} d^3x \left[1 + \mathcal{O}(y^2/\lambda^2)\right] \\ &= -KV_d \operatorname{sech}^2(q/\lambda) + \mathcal{O}(KV_d(R_0/\lambda)^2). \end{aligned} \tag{B5}$$

Let the easy axis for the magnetic anisotropy lie along the z-axis. Then

$$\begin{aligned} U_{anis}(q) &= \left[\int_R^3 - V_d - \int_R^3\right] K\left(\hat{m}_x^2 + \hat{m}_y^2\right) = -K\int_{V_d} d^3x \operatorname{sech}^2\left(\frac{y-q}{\lambda}\right) \\ &= -KV_d \operatorname{sech}^2(q/\lambda) + \mathcal{O}(KV_d(R_0/\lambda)^2). \end{aligned} \tag{B6}$$

The contribution from the demagnetization energy requires a little more work. As discussed in appendix A, the void has a magnetic 'charge' induced on its surface S_d which produces a demagnetization field H_d outside the void. This gives rise to a demagnetization energy

$$E_{demag} = -\frac{1}{2}\int_R^3 - V_d \; d^3x \; M_w \cdot H_d. \tag{B7}$$

As the static Bloch wall configuration (appropriate when the void is absent) has zero demagnetization energy, we have

$$U_{demag}(q) = -\frac{1}{2}\int_R^3 - V_d \; d^3x \;\; M_w \cdot H_d. \tag{B8}$$

The demagnetization field H_d satisfies

$$\nabla \times H_d = 0 \qquad \nabla \cdot (H_d + 4\pi M_w) = 0$$

subject to the boundary condition that $|H_d(x)| \to 0$ as $|x| \to \infty$. The solution is $H_d = -\nabla\Phi_d$, where

$$\Phi_d = \oint_S \frac{\hat{n}' \cdot M_w(x') \; da'}{|x - x'|} - \int_R^3 - V_d \; d^3x \frac{\nabla \cdot M_w(x')}{|x - x'|} = -\oint_{S_d} \frac{\hat{x}' \cdot M_w(x') \; da'}{|x - x'|}. \tag{B9}$$

Here $S = S_\infty \cup S_d$. For $R_0 \ll \lambda$, M_w is constant over S_d and given by

$$M_w(\mathbf{0}) = M(\operatorname{sech}(q/\lambda), 0, -\tanh(q/\lambda)) \equiv M\hat{m}. \tag{B10}$$

Using (B10) in (B9) and expanding $|x - x'|^{-1}$ in spherical harmonics gives

$$\Phi_d(x) = -\frac{MV_d}{r^2}\hat{m}\cdot\hat{x} \tag{B11}$$

so that

$$H_d = \frac{MV_d}{r^3}\left[\hat{m} - 3\hat{x}(\hat{m}\cdot\hat{x})\right]. \tag{B12}$$

We see that H_d is a pure dipole field outside the void. Simple algebra gives

$$\begin{aligned} M_w \cdot H_d = (M^2V_d/r^3)\big[&\left(3z^2/r^2 - 1\right)\tanh(q/\lambda)\tanh \\ &\times((y-q)/\lambda) + \left(1 - 3x^2/r^2\right)\operatorname{sech}(q/\lambda)\operatorname{sech}((y-q)/\lambda) \\ &+(3xz/r^2)\{\tanh(q/\lambda)\operatorname{sech}((y-q)/\lambda) \\ &-\operatorname{sech}(q/\lambda)\tanh((y-q)/\lambda)\}\big]. \end{aligned} \tag{B13}$$

To evaluate the integral in (B8) it proves convenient to adopt cylindrical coordinates (ρ, α, y). Here (ρ, α) are polar coordinates for the xz-plane. The α-integral of the term in (B13) proportional to xz/r^2 vanishes and will be dropped from further consideration. Thus

$$\begin{aligned} U_{demag}(q) = -\frac{1}{2}\int_{-\infty}^{\infty} dy \int_{\rho_m^2(y)}^{\infty} \frac{1}{2}\, d\rho^2 \int_0^{2\pi} d\alpha \frac{M^2V_d}{(y^2+\rho^2)^{3/2}} \\ \times\left[\left(3\rho^2\cos^2\alpha/(y^2+\rho^2) - 1\right)\tanh(q/\lambda)\tanh((y-q)/\lambda)\right. \\ \left.+\left(1 - 3\rho^2\sin^2\alpha/(y^2+\rho^2)\right)\operatorname{sech}(q/\lambda)\operatorname{sech}((y-q)/\lambda)\right] \end{aligned} \tag{B14}$$

where

$$\rho_m^2(y) = \begin{cases} 0 & |y| > R_0 \\ R_0^2 - y^2 & |y| \leqslant R_0. \end{cases} \tag{B15}$$

The α-integral is trivial and the ρ^2-integral can be done by parts. Carrying out these integrations gives

$$\begin{aligned} U_{demag}(q) &= -\frac{\pi}{2}M^2V_d\int_{-\infty}^{\infty} dy\left[\tanh(q/\lambda)\tanh\left(\frac{y-q}{\lambda}\right) - \operatorname{sech}(q/\lambda)\operatorname{sech}\left(\frac{y-q}{\lambda}\right)\right] \\ &\quad\times\frac{\rho_m^2(y)}{(y^2+\rho_m^2(y))^{3/2}} \\ &= -\frac{\pi}{2}\frac{M^2V_d}{R_0^3}\int_{-R_0}^{R_0} dy\,(R_0^2 - y^2)\left[\tanh(q/\lambda)\tanh\left(\frac{y-q}{\lambda}\right)\right. \\ &\quad\left.-\operatorname{sech}(q/\lambda)\operatorname{sech}\left(\frac{y-q}{\lambda}\right)\right] \\ &= -\frac{\pi}{2}\frac{M^2V_d}{R_0^3}\int_{-R_0}^{R_0} dy\,(R_0^2 - y^2) \\ &\quad\times\left[\frac{\tanh(y/\lambda)\tanh(q/\lambda) - \tanh^2(q/\lambda) - \operatorname{sech}^2(q/\lambda)\operatorname{sech}(y/\lambda)}{1 - \tanh(y/\lambda)\tanh(q/\lambda)}\right]. \end{aligned} \tag{B16}$$

Since $|y| \leqslant R_0 \ll \lambda$, we expand the hyperbolic functions to second order in (y/λ). This gives

$$U_{\text{demag}}(q) = \frac{\pi}{2}\frac{M^2 V_d}{R_0^3}\int_{-R_0}^{R_0} dy\ (R_0^2 - y^2)\left[-1 + \left(1 - \frac{1}{2}\text{sech}^2(q/\lambda)\right)(y/\lambda)^2\right]$$
$$= -\frac{KQ^{-1}V_d}{4}\left[-\frac{4}{3} + \frac{4}{15}\left(\frac{R_0}{\lambda}\right)^2\left(1 - \frac{1}{2}\text{sech}^2(q/\lambda)\right) + \mathcal{O}\left(\frac{R_0^4}{\lambda^4}\right)\right]. \quad \text{(B17)}$$

We see that the leading term is constant and does not contribute to the pinning force. What is more, the overall magnitude of U_{demag} is proportional to $Q^{-1} \ll 1$ so that it is small compared to U_{exc} and U_{anis} and will not contribute significantly to $U(q)$. Thus

$$U(q) \approx U_{\text{exc}} + U_{\text{anis}} = -2KV_d\,\text{sech}^2(q/\lambda) \equiv -U_0\,\text{sech}^2(q/\lambda) \quad \text{(B18)}$$

where $U_0 = 2KV_d$. If, for example, we assume $U_0 \equiv 0.1$ eV, and that our magnetic insulator is LaGaYIG, so that $Q = 25.2$, and $K \simeq 2000$–3000 erg cm^{-3}, then $R_0 \simeq 150$–200 Å, which gives the value used in the macroscopic domain wall calculation. Similiar algebra using the appropriate value of U_0 (see section 2) yields the value of R_0 used in the mesoscopic domain wall calculation.

References

[1] Stamp P C E, Chudnovsky E M and Barbara B 1992 *Int. J. Mod. Phys.* B **6** 1355
[2] Chudnovsky E M and Gunther L 1987 *Phys. Rev. Lett.* **60** 661; 1988 *Phys. Rev.* B **37** 9455
[3] Van Hemmen J L and Süto S 1986 *Europhys. Lett.* **1** 481; 1986 *Physica* B **141** 37
Enz M and Schilling R 1986 *J. Phys. C: Solid State Phys.* **19** 1765, L711
[4] Barbara B and Chudnovsky E M 1990 *Phys. Lett.* **145A** 205
[5] Awschalom D D, McCord M A and Grinstein G 1990 *Phys. Rev. Lett.* **65** 783
[6] Awschalom D D *et al* 1992 *Phys. Rev. Lett.* **68** 3092
[7] Stamp P C E 1991 *Phys. Rev. Lett.* **66** 2802
[8] Chudnovsky E M, Iglesias O and Stamp P C E 1992 *Phys. Rev.* B **46** 5392
[9] Giordano N and Monnier J D 1993 *Proc. 20th Int. Conf. on Low Temperature Physics (Eugene, OR, 1993); Physica* B at press
[10] Paulsen C *et al* 1992 *Europhys. Lett.* **19** 643
[11] Zhang X X *et al* 1992 *J. Phys.: Condens. Matter* **4** L163
[12] Caldeira A O and Leggett A J 1983 *Ann. Phys.* **149** 374; 1984 *Ann. Phys.* **153** 445
[13] Leggett A J 1980 *Prog. Theor. Phys. Suppl.* **69** 80
[14] Schrödinger E 1935 *Naturwissenschaften* **23** 807
[15] Malozemoff A P and Slonczewski J C 1979 *Magnetic Domain Walls in Bubble Materials* (New York: Academic)
[16] Leggett A J *et al* 1987 *Rev. Mod. Phys.* **59** 1
[17] Dissipation via environmental nuclear spins has also been considered for the case of magnetic particles in Garg A 1993 *Phys. Rev. Lett.* **70** 1541; 1994 *J. Appl. Phys.* submitted
This effect has not been explicitly examined for the case of domain wall quantum coherence although the first of these references suggests that this effect will be important in this case as well. Careful sample preparation is crucial to minimizing this effect. The reader is referred to the above references for further discussion.
[18] Press W H *et al* 1990 *Numerical Recipes: The Art of Scientific Computing* (New York: Cambridge University Press)